Research Article | Vol. 29, No. 4 / 15 February 2021 / Optics Express 5694

Optics EXPRESS

Stabilization of the 81-channel coherent beam combination using machine learning

DAN WANG,* QIANG DU, TONG ZHOU, DERUN LI, AND RUSSELL WILCOX

Lawrence Berkeley National Lab, 1 Cyclotron Road, Berkeley, CA 94720, USA
*dwang2@lbl.gov

Abstract: We develop a rapidly converging algorithm for stabilizing a large channel-count diffractive optical coherent beam combination. An 81-beam combiner is controlled by a novel, machine-learning based, iterative method to correct the optical phases, operating on an experimentally calibrated numerical model. A neural-network is trained to detect phase errors based on interference pattern recognition of uncombined beams adjacent to the combined one. Due to the non-uniqueness of solutions in the full space of possible phases, the network is trained within a limited phase perturbation/error range. This also reduces the number of samples needed for training. Simulations have proven that the network can converge in one step for small phase perturbations. When the trained neural-network is applied to a realistic case of 360 degree full range, an iterative scheme exploits random walking at the beginning, with the accuracy of prediction on phase feedback direction, to allow the neural-network to step into the training range for fast convergence. This neural-network-based iterative method of phase detection works tens of times faster than the commonly used stochastic parallel gradient descent approach (SPGD) using a single-detector and random dither when both are tested with random phase perturbations.

1. Introduction

Coherent beam combination is a way to derive high energy and power from lasers which are limited in output, by adding outputs together [1,2]. We are using this approach to produce high energy pulses from fiber lasers, with a goal of combining about 100 lasers with 10 mJ each to produce Joule-level, ultrafast pulses [3,4]. We choose to combine on a diffractive optical element (DOE) to reduce the number of optics each beam must go through, with two elements per beam needed to combine ultrafast pulses while minimizing dispersion [5–7].

An essential task in beam combination is to actively control the input beam phases, which are subject to mechanical and thermal perturbations, maintaining the correct phasing to maximize combination efficiency. There are several methods of determining phase errors to facilitate feedback. One uses a secondary interferometer to read the phases directly by interfering a reference beam with each input beam, but this device must also be stable, and adds to the number of optics [8,9]. Another approach, most commonly used, is to measure only the combined beam power and dither the input phases using a genetic algorithm; stochastic parallel gradient descent (SPGD) [10,11]. This works for CW and high repetition rate pulsed combination, but the number of steps (feedback cycles) it takes to converge is approximately ten times the number of combined beams [12]. If there is one sample point per pulse, and one step or fewer per sample point, this process becomes too slow for combination of pulses with kHz repetition rates and hundreds of beams, which is our situation. SPGD is hampered by gaining information from only one detector, giving no indication of which beam or which direction to adjust, and it also introduces noise by its dithering and searching process [13].

After the DOE, an array of uncombined beams adjacent to the combined one emerges. These are always present at low intensity, even when combining is optimal. For a one-dimensional,

#414985 https://doi.org/10.1364/OE.414985
Journal © 2021 Received 7 Dec 2020; revised 26 Jan 2021; accepted 27 Jan 2021; published 8 Feb 2021

Optics EXPRESS

N-way combiner, since each of N input beams is split by the combiner at the same time it adds the N beams together, there will be N sets of N uncombined beams each, all having one common point which is the combined center beam. Thus, there are $2N-1$ diffracted beams. For a two-dimensional combiner with $N \times M$ beams, the dimensions are orthogonal, and the total is $(2N-1)\times(2M-1)$. This can be seen as a spatial convolution process [6,13]. Since the diffracted beams overlap and interfere at many points (more than the number of input beams), the resulting interference pattern can potentially indicate relative phases of the input beams. It is possible to measure this interference pattern with a camera and use this information to derive phase errors, but since only intensities are measured, phase information is lost and must be retrieved somehow. This is a classic problem when analyzing interference patterns, usually solved by an iterative process which converges after much computation, which tends to be slow [14]. While phase retrieval applied to analysis of static patterns (e.g. X-ray crystallography) is adequate, a dynamic feedback system requires quick determination of phase errors, so a more efficient solution must be sought.

If the interference pattern can be interpreted to yield phase information, we would expect that a pattern recognition machine which can learn the mapping from pattern to phase could yield the phase errors directly. It can be trained by presenting it with patterns theoretically derived from a set of randomly chosen phases, as a "labeled" training data set, and tested by another known data set, to build the map between diffraction pattern intensity and phase error.

This can be realized using a neural network (NN), with input and output layers, and internal layers which connect them using variable strength connections that change during training [15–17]. In this paper, we seek to validate this method by making it work on a simulation before applying it to an actual combiner, showing it can at least work in an ideal situation before introducing other types of error.

An important question arises: are the patterns uniquely mapped onto input phases or not? Certainly, if we consider the case of two beam interference, there will be two cycles of intensity variation per one 360 degree cycle of phase rotation. This means the inferred phase is ambiguous, with no unique solution. Even if a phase-shifted interference pattern is also generated, and there can be in-phase and quadrature-phase signals, which-way information is generated without resolving the 180 degree phase ambiguity. Nevertheless, we have observed a small, 8-beam DOE combiner which allows derivation of input beam phases directly from interference spot intensities [13], so we may hope this can be done for larger beam counts.

In fact, testing a two-dimensional, $9 \times 9 = 81$ beam DOE combiner [18,19], we observe several, nearly identical interference patterns resulting from very different beam phases. Thus, the solutions to the problem of phase retrieval are not unique for this particular example. If the phase errors are small enough to be inside one "fringe" (less than 180 degree range) there is no ambiguity, training the NN is possible, and it works to identify the phase errors directly, allowing for error correction in one step. Outside this limited range, the NN is confused and cannot be trained.

This implies two different approaches may be needed; the usual case is correction of small perturbations and this can be performed by the NN, while full recovery from a random state is infrequent and could be slower. However, we have found that the NN trained in a limited range works over the full range of errors anyway, because there is a better than even chance that it will go in the right direction, and this probability improves the closer it gets to the training range. Once it has random-walked downhill, so to speak, it falls into the unambiguous region and quickly and robustly locks to the optimum point. Even with this initial random walk, the NN is tens of times faster than SPGD using a single-detector and random dither, which we show in side-by-side simulations.

In the sections below, these topics are explained in detail.

Optics EXPRESS

2. Model of diffractive combining and basis of pattern recognition with the NN algorithm

This section shows the physical model of spatial convolution with the DOE, and discusses the principle of interference pattern recognition with a NN algorithm which learns the mapping from pattern to phase, thus yielding the phase errors directly. We found a phase ambiguity in our problem in the 360 degree range, which requires training of the NN within a limited phase perturbation range and with a reduced number of samples.

2.1. 81-way 2D diffractive combining using a 9×9 DOE

The physical process of 2D diffractive combining can be represented as a discrete 2D convolution shows below [6,13,20]:

$$\begin{aligned} s(i,j) &= \sum_{k=-\infty}^{\infty} \sum_{l=-\infty}^{\infty} b(i,j)d(i-k,j-l) \\ &= b(i,j) * *d(i,j) \end{aligned} \tag{1}$$

where $b(i,j)$ is the input beam function, $d(i,j)$ is the intrinsic DOE transmittance function, and $s(i,j)$ is the far field amplitude of the diffracted beam, all being complex. i,j,k,l are integers, where (i,j) is the horizontal and vertical coordinate of both the input beam array, and the far field diffracted beam array from the incident direction, with zero-order beam located at (0,0).

As shown in Fig. 1, for an input of 9×9 beams, with $i,j \in [-4,-3,\ldots,0,\ldots,3,4]$, the output will be 17×17, because each input beam produces 9×9 outputs, always overlapped at the center beam. In general, as 2D convolution suggests, for $N \times N$ inputs and $N \times N$ shaped $d(i,j)$, there will be $(2N-1) \times (2N-1)$ outputs.

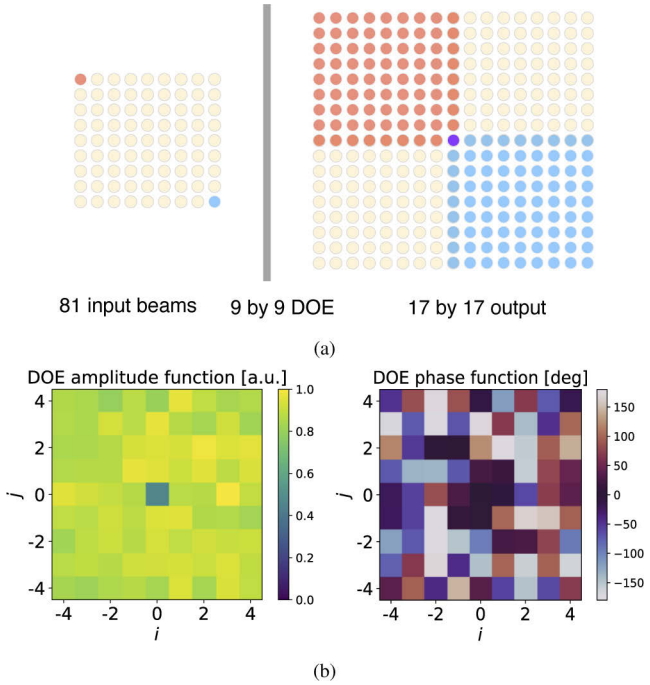

Fig. 1. (a) How two beams in the 9×9 input array contribute to the 17×17 output array, while overlapping at the center. (b) Measured amplitude and phase function of a 9×9 DOE used in the modeling. Amplitude function is amplitude transmission efficiency, and phase function unit is degree. i and j are indices on x and y axes.

Optics EXPRESS

Once we have the intrinsic DOE function $d(i,j)$, we can predict interference patterns given any arbitrary input base on Eq. (1). In order to perform actual measurements on a 9×9 diffractive combiner without incurring the cost and complexity of building a phase-controlled beam array using discrete optics, we opted to generate a beam array using a spatial light modulator [18,19]. This provides for control of all parameters of each beam, enabling measurements of the actual DOE phase function and tests of combining and control. The measured intrinsic DOE function $d(i,j)$ including the amplitude function and the phase function in our model were found experimentally and are shown in Fig. 1(b), with x-axis and y-axis grids representing the integers i and j.

In this work, we define one power unit as the power of one diffracted spot after the DOE, when one beam is incident. This will be 1/81 of the incident beam power. When the 81 beams are optimally combined, the output power in the central beam will be 81 times the power of one input beam, and 81^2 times the power of our defined power unit. The increase in central beam power as beams are added is quadratic, as the side spots diminish in power at the same time the central one is augmented [19].

Optimal combining requires the input beam phase condition as: $\angle b(i,j) = -\angle d(-i,-j)$, where $\angle$ stands for the phase function. This means that the ideal input laser beam phase array, which provides for optimal combining, has to match the DOE intrinsic phase function [6,13]. When input laser phase $b(i,j)$ is other than ideal, there will be excess loss, i.e., combining efficiency drops with phase errors.

Our stabilization goal for phase control requires to achieve <1% efficiency loss. The function of coherent combining efficiency loss versus piston phase error is [21]:

$$1 - \eta = \sigma_\phi^2 \tag{2}$$

where η is the combining efficiency normalized to the maximum achievable efficiency of the DOE, and σ_ϕ is the uncorrelated RMS laser phase error from each channel, in radians. Equation (2) indicates that our stabilization goal is to control σ_ϕ<6 degrees in order to achieve η>99%.

2.2. Mapping from interference pattern to phase with the NN algorithm

It is necessary that the control system recover optimal beam phasing from a random input, and maintain that in the presence of slow and fast phase perturbations. We would like to deconvolve the factors in Eq. (1), so that we can find the errors in $\angle b(i,j)$, given the known phase function $\angle d(i,j)$ and the measured amplitude $s(i,j)$.

Due to the lack of optical phase information from far field detectors such as a camera or photodiode arrays, the mapping between the 17×17 far field interference pattern $|s|^2$ and the 9×9 input beam phases $\angle d$ cannot be solved directly. A typical iterative phase retrieval method would be too slow for active feedback, and sensitive to measurement errors [14]. This kind of deterministic mapping problem has been shown to be solvable by machine learning algorithms [15,22,23]. Here, we apply machine learning to derive phases from far field interference patterns, to quickly find phase errors to correct.

For the interference pattern recognition, the artificial neural network is used to find the mapping function between the interference patterns and the laser phase errors, which is achieved by training the network with interference patterns with known phase perturbation. Once the mapping function is identified, the neural network can recognize a pattern and find the corresponding phase errors for any given pattern within one step.

The architecture of the NN we choose (as shown in Fig. 2) has an input layer with 285 neurons ($17 \times 17 - 4$, with 4 unchanging corner spots removed), which represent the interference pattern, and two inner hidden layers with 400 and 200 neurons respectively.We choose these numbers experimentally to adequately represent the data while avoiding unnecessary complexity, but we have not optimized them. The output layer comprises the predicted 81 beam phases. A neuron is

Optics EXPRESS

connected to many inputs, which generates an output signal when the inputs exceed a certain threshold. The neuron is mathematically a summation of all the input signals multiplied by a weight matrix which describe the mapping function. The weight matrix determines the sensitivity of the neuron to each input. The training of the network is the adjustment of the sensitivity of the neuron to each of its inputs. As the network is trained, the weights for each neuron in the network are adjusted to change the output of the neural network to match it with the true output (the known phase perturbation) [16].

We also tested NN architecture with an input layer of 284 neurons, dropping the center combined beam because of camera saturation. When the feedback is operating near optimal, we would use the full dynamic range of the camera to capture only the side beam pattern. We found that the pattern recognition performance using such incomplete information is the same as for 285 input neurons. For the inner layers, there are no fixed rules or formulas on how the architecture is selected [24], since it depends on the complexity of the problem. We follow common practice and insert two inner layers, tuning the number of neurons to reach the required training error while maintaining a reasonable number of training samples.

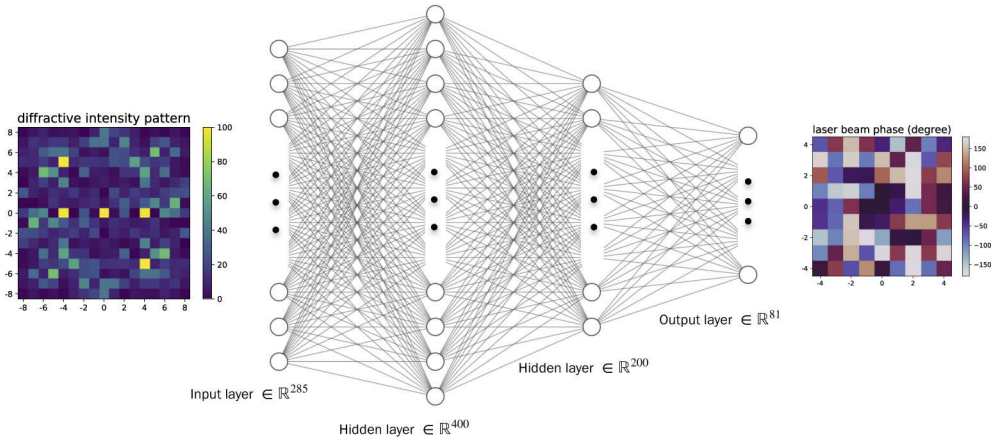

Fig. 2. Structure of the neural network, with interference patterns (17×17) as input and the corresponding 81-beam phases array (9×9) as the output.

2.3. *Ambiguity of solutions: the impact on phase prediction*

In a simple interference of two beams, for example, one beam working phase is fixed at 90 degree, and the other beam phase θ is varied, the output intensity will be $S = |1 + \cos(\theta - 90)|^2$. To obtain a mapping function of amplitude to phase, $\theta = \arccos(\pm\sqrt{S} - 1) + 90$, θ is a monotonic function of S only if θ is in the range of -90 to 90 degree. And solutions are ambiguous in the full phase range of 360 degree.

Figure 3 shows what happens when training the NN to predict the input phase offset based on observed intensity for the above two beam example. Multiple solutions appear beyond $\theta = \pm 90$ degree. Figure 3(a) indicates that the NN works well if we train it in a limited range which guarantees a monotonic output, i.e., the predicted value agrees with the real phase values for any test data, which follows the curve with slope of $k = 1$ (red dashed curve). Figure 3(b) shows that the NN becomes confused when trained in the full phase range. The predicted phase data looks like a bow-tie with the center at $\theta = \pm 90$ degree where non-unique solutions appear. Because the curve of intensity S is symmetric about the tie-center point of 90 ± 45 degree, the prediction points fill all the areas in between the curve with slope $k = 1$ (red dashed curve) and the curves with slope $k = -1$ (blue dashed lines).

Optics EXPRESS

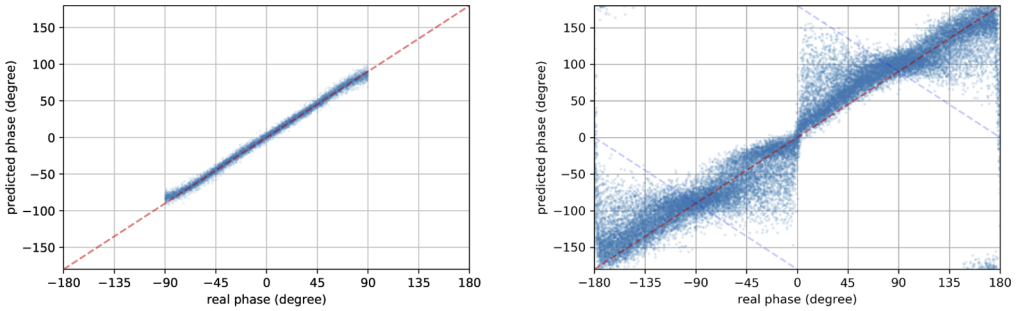

(a) (b)

Fig. 3. The consequences of non-uniqueness. Predicted phase versus real phase when trained in a limit range of $[-90, 90)$ degree (a) and (b) in the full range of 360 degree.

Non-unique solutions also exist in the more complex 81-beam combination problem. We used our model of the combiner and entered random input phases to produce corresponding 17×17 output intensity patterns. We then scanned the input beam phase space to find a similar output intensity pattern, comparing them in amplitude while also comparing the input phases.

Three example cases are shown in Fig. 4, with the left column showing three randomly chosen output interference patterns. The second column shows similar patterns found by scanning and searching. The third column shows small intensity differences between the random given pattern and the searched pattern. However, the last column shows the input phase difference between the given and searched examples, revealing that they are not at all similar. (Note that the upper limits of the color bars for the intensity patterns are only up to 100 in the plots for high contrast images. This is in order to see the patterns clearly, while the output power in the central beam can reach up to 81^2 times the power of our defined power unit).

Figure 4 indicates that quite different input beam phases correspond to almost indistinguishable interference patterns, so that the difference between patterns can be within practical measurement error. Although this is not a strict mathematical proof of non-uniqueness, it is apparent that there is no clear one-to-one mapping from interference pattern to phase over the full range of phases,which was also found to be true in Ref. [23]. Because of this, the NN cannot be trained on the 81-beam combiner over the full range. Indeed, when we have attempted to do so, the NN prediction error never converges to a low value.

2.4. *Numerical results of the NN when trained in a limited phase perturbation range*

During optimization of the network, the measure of success is the root mean square error (RMSE), defined as

$$RMSE = \sqrt{\frac{1}{n}\sum_{i=1}^{n}(Y_i - O_i)^2} \tag{3}$$

where O_i is output from the NN and Y_i is the real/target value. As discussed in Section 2.1, RMSE is required to be within σ_ϕ and less than 6 degrees in order to maintain combining efficiency above 99% [19]. During training, we divide our dataset into two subsets. The first is the learning dataset, also called "training samples", i.e., a subset to train a model. The second is the test dataset, which is a subset that the NN hasn't seen before in order to test the predictive performance of the trained model. While the RMSE of a network for a learning dataset gradually decreases with number of samples, predictive performance of the network on test dataset has parabolic dependence for large number of samples. This is because a network with a sufficient number of neurons in the hidden layer can exactly implement an arbitrary training set, and it can

Optics EXPRESS

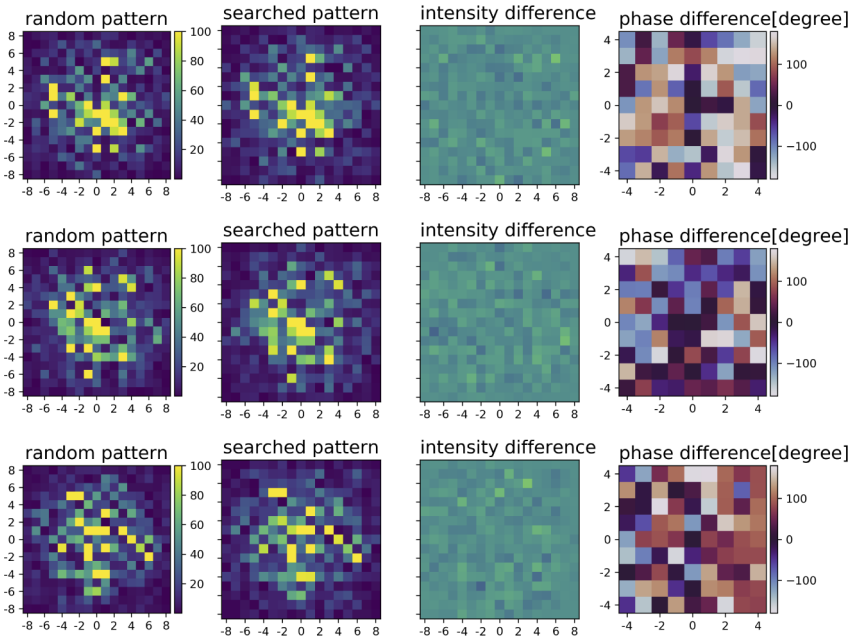

Fig. 4. Similar 17×17 interference patterns with slight intensity differences (left two columns, with difference in third column) correspond to very different 9×9 beam phases, as shown in the right most column, in degrees.

learn both the desired information and noise that will lower the predictive ability of the network [25].

We trained the network with phase perturbations over a range of ±40 degree, with 0.5 million simulated example samples, and found that it can predict phase within RMSE of 4.6 degree for test dataset as shown in the yellow curve of Fig. 5. The RMSE for the learning dataset is smaller than the RMSE for the test dataset, indicating that the NN structure is complicated enough to learn the relation between the input and output, while the prediction capability is mainly limited by the number of samples.

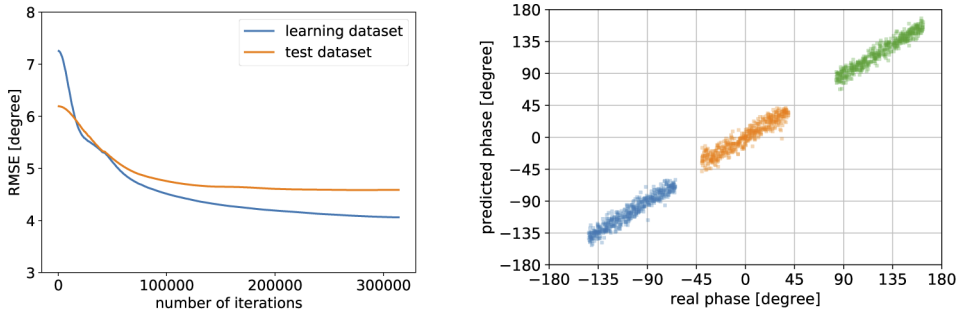

(a) (b)

Fig. 5. (a): the root mean square error (RMSE) of the NN for learning samples and test samples. (b): performance of the trained NN on the test dataset.

We randomly generated 500 random test samples, with the NN-predicted phase versus the real phase shown for 3 of the input beams (out of 81) in Fig. 5(b). Different colors represent the

Optics EXPRESS

different beams, all centered at the optimal phase for highest combining efficiency, for input errors over a range of ±40 degree. All the dots line on a straight line, with a variance corresponding to an RMSE value of 4.6 degree. This is based on the same test dataset as in Fig. 5.

Table 1 shows the number of examples used for different ranges of input phase errors. We found that for all cases the RMSE for the test dataset decreases as the number of samples increases, reaching a minimum at very large numbers of samples. We increased the number of training samples in the larger training ranges of ±80 degree and ±90 degree in order to reduce the test RMSE for these cases. Still, the RMSE increases for larger phase error ranges. When trained over a range larger than 180 degrees, the NN prediction accuracy actually worsens with training, as it is now confused by non-unique solutions.

Table 1. Number of samples used in training the neural network with different phase perturbation ranges, and smallest RMSE.

input phase error range [degree]	samples used to train the NN	RMSE for test dataset [degree]
±20	50,000	2.1
±40	50,000	3.9
±60	50,000	7.8
±80	100,000	14.1
±90	200,000	19.8

Note that we are using the NN model of training range of ±40 degree for all the subsequent NN applications if not specified.

3. NN application to feedback control

In this section we validate the NN algorithm as part of a feedback control loop as a phase detector. As discussed above, the NN trained in the limited phase range implies there could be two different approaches to feedback: the usual case of correction of small perturbations within training range in one step, and full recovery from a random state, which is infrequent and slower. A different algorithm could be used for the second case. However, we show that the NN trained in a limited range works over the full range of errors, removing the need for a second approach.

3.1. One-step feedback for small phase perturbations

Figure 6 shows how the algorithm based on a neural-network and iteration is accomplished in the feedback loop, with one whole cycle around the loop counting as one feedback step. With an interference pattern fed into the NN, it then recognizes the phase error and applies a phase correction in order to go toward the ideal phase. The laser beams' phase is then updated, and a new interference pattern is generated, and so on. Once the phase matrix is close to the optimal point, i.e.,within the RMSE of 6 degrees, the phase correction from the NN recognition algorithm is always less than the RMS phase error, i.e., always keeping the optimal/stable state within a given tolerance during the iterative process.

For fast phase perturbations within the training range, the stabilisation feedback loop only takes one step to recover, as shown in Fig. 7. Arbitrary phase perturbation within the training range of ±40 degree is introduced, leading to a non-optimally combined pattern and relatively poor combining efficiency less than 95%. The interference pattern is taken by the NN as input for predicting the phase perturbation for correction, and the correction is able to recover to >99% of optimal combining efficiency and then always remain stable.

Optics EXPRESS

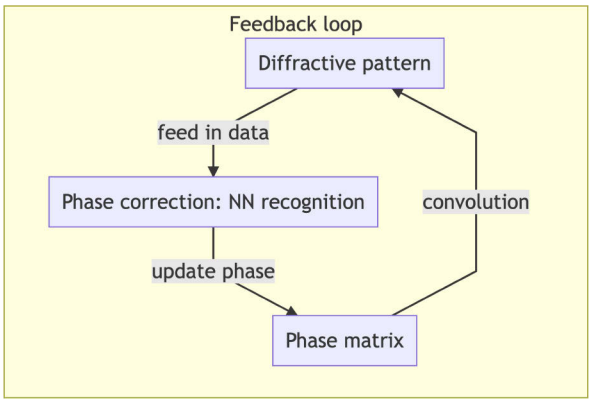

Fig. 6. Iterative feedback loop based on the neural-network.

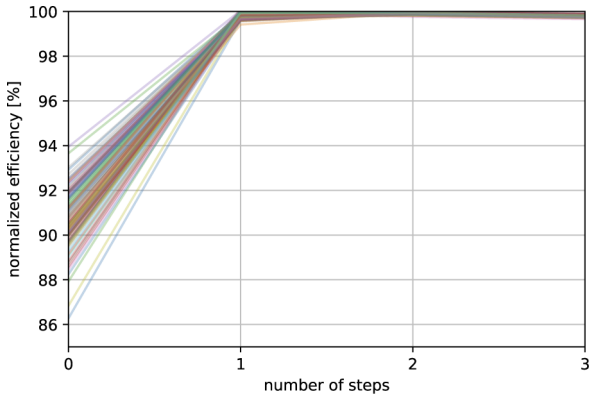

Fig. 7. One step feedback when phase perturbation is in the training range. 100 random cases are shown.

3.2. *Application in the full range with an iterative process*

We now apply the feedback loop in Fig. 6 with the NN model trained in ±40 degree range to the full phase perturbation range of $[-180, 180]$ degree, which can perform well due to an iterative process where successive correction steps move the phase error toward the goal. The controller random-walks the system into locking range in a few steps, before reaching near-optimal combining state in a single step, then maintains the efficiency loss to be <1% thereafter. The probability that a random walk will land inside the training range, and the dependence of the prediction accuracy on the initial state will be discussed in Section 4.1.

As shown in Fig. 8, it takes multiple steps for an arbitrary phase perturbation in the 360 degree range to reach the optimal point. Statistically, 99.5% of 50,000 random testing cases are able to converge (i.e. reach 99% of theoretical η) within 100 steps, with the majority of them less than 40 steps.

Figure 9 shows the NN phase prediction error, i.e., $O_{i,j} - Y_{i,j}$, where $O_{i,j}$ and $Y_{i,j}$ are the output from the NN and the real value respectively. Snapshots of the error are taken at a series of iterative steps for a random case which has a relatively large phase error at the first step. The error reduces rapidly with successive steps. Final prediction error is within the prediction RMS error of 5 degree for all the beams.

Optics EXPRESS

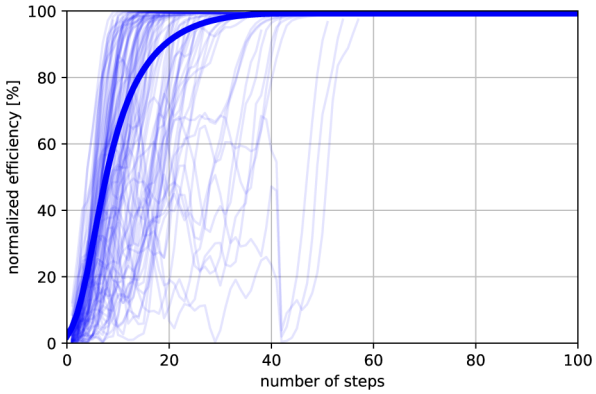

Fig. 8. Normalized combining efficiency versus number of correction steps, when phase perturbation is in the 360 degree range. 100 random cases and the average (red solid line) are shown.

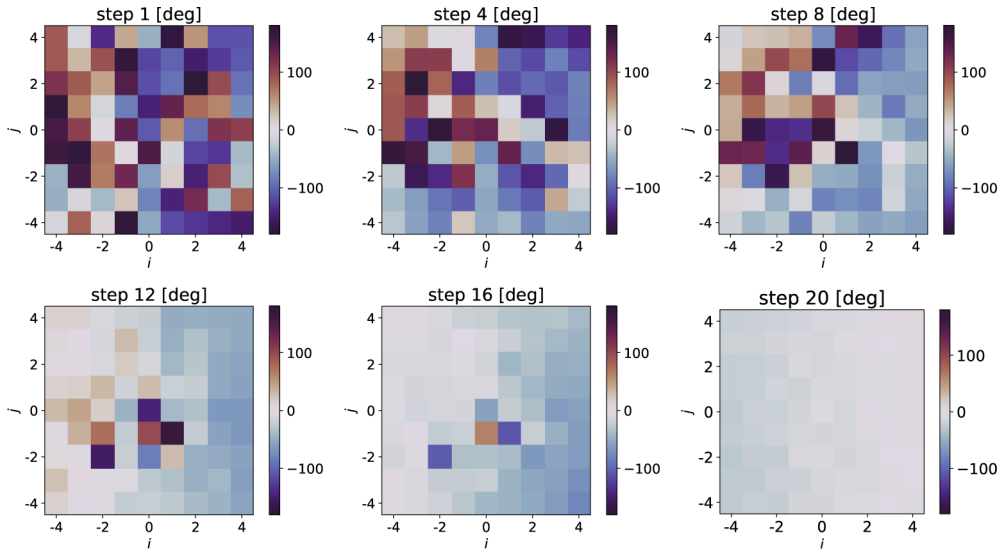

Fig. 9. NN prediction error for the input beam phase (9×9) array at different iterative steps for a typical random case.

4. Why limited range training is adequate for full range operation

This section discusses why the NN algorithm works in the full phase perturbation range, by looking at the accuracy of the NN prediction model outside the training range, and how the initial random walk improves the probability of getting phases closer to the training range. We also compare the NN algorithm with the traditional SPGD algorithm, showing that the NN is tens of times faster than SPGD using a single-detector and random dither with side-by-side simulations.

4.1. Reason of convergence of the NN-based feedback loop

Here we use statistics to indicate the reasons why the iterative method based on NN prediction can bring arbitrary phase errors in the 360 degree range back to optimal states. We first introduce the concept of accuracy ratio, which is defined as the percentage of NN predictions that move toward the goal. Accuracy ratio also corresponds to the possibility for one beam to go back to the

Optics EXPRESS

optimal phase. When calculating the accuracy ratio based on many cases, if the phase distance to the working phase of one beam is closer compared to the original value for a given run, we take the accuracy flag as true for this beam for this run, otherwise the flag as false. We then count the overall accuracy ratio over multiple runs. For a completely random guess the accuracy ratio is 50%.

$$\text{accuracy ratio} = \frac{\sum(\text{case of beam phase getting closer to optimal})}{\text{total cases}} \tag{4}$$

The accuracy of the NN prediction model over the full error range for one prediction step is shown in Fig. 10. The model is trained in the phase perturbation range with absolute value of 40 degrees, thus there is 100% accuracy within the training range.

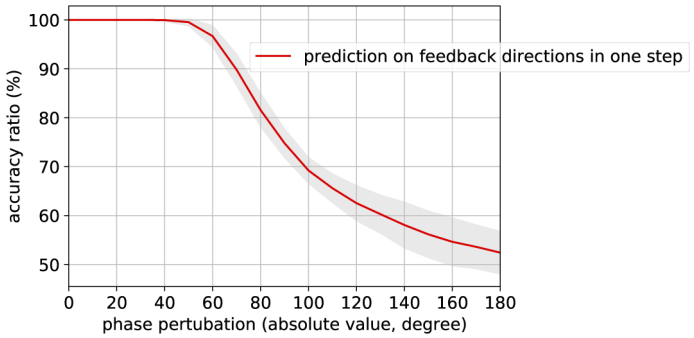

Fig. 10. Accuracy of the NN prediction model in and outside the training range with 1 feedback step.

The accuracy ratio is still slightly higher than 50% when the phase perturbation is in the full range of $[-180, 180]$ degree which means that first guesses will likely be in the right direction. Any movement toward the goal improves this probability, making this a random walk downhill, until the training range is reached, and the goal is hit in one step.

The iterative process acts as a search, automatically. The probability of beams to move closer to the optimal phase keeps rising as the iterative process proceeds as shown in Fig. 11. We found that the curve of accuracy ratio versus the number of feedback steps (blue curve with green areas as the deviation) is following a logistic function-like curve (red curve). This function has been used to model population growth, and is a common S-shaped curve (sigmoid curve) with equation $y = \frac{L}{1+\exp^{-k(x-x_0)}}$, where x_0 is the x value of the sigmoid's midpoint; L, the curve's maximum value; and k, the logistic growth rate or steepness of the curve [26–29]. The random walk downhill model, with accuracy ratio increasing when the prediction is closer to the training range, helps produce exponential growth initially. The RMSE from the NN model limits the final accuracy ratio values, leading to the saturation value of $L = 93$ in Fig. 11, and around the optimal phase the predictions have larger deviations. Still, the overall RMSE is still within 6 degrees, thus combining efficiency can reach 99% as shown in Fig. 8.

Figure 12 shows the convergence curves of one beam's phase in the iterative process. During 1000 runs with random initial state in the full phase range, most of the cases converge after tens of steps. The saw-tooth behavior seen in the figure is due to phase wrapping, which is not just an artefact of the way the data is presented, but a phenomenon that helps the system find the training range and lock in to a robustly optimal state. We have specially picked 3 random cases in Fig. 12 to show different convergence paths. The magenta curve always keeps the right direction and converges within 10 steps. The red curve had a wrong direction at the beginning and bounces around for about 10 steps but finally converges, because as the process is applied iteratively, so that the new, wrong state is the basis of a new prediction, the resulting random walk quickly finds the training range. For most cases it is not possible to go far in the wrong direction, as phase is

Optics EXPRESS

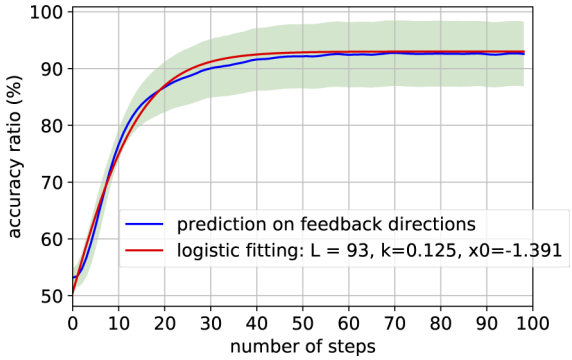

Fig. 11. Accuracy improvement with iterative process for cases with random initial beam phase in the full range.

cyclic. If the system goes too far in the wrong direction, it becomes the right direction again, as the red curve illustrates. We also have some cases like the green one shown in the figure that doesn't converge after 50 steps, although this is a rare case, and will almost certainly converge before 100 steps.

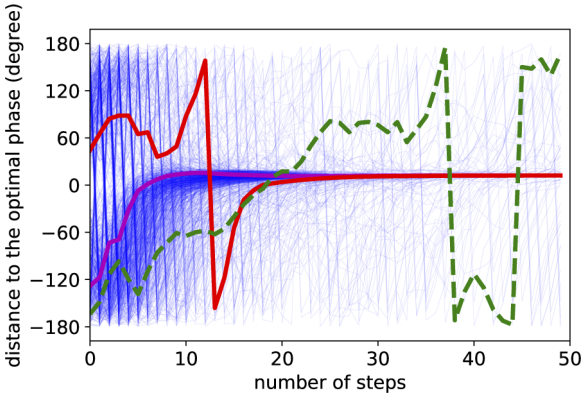

Fig. 12. 1000 cases of a random beam phase converged in the iterative process. Most of the cases converge after tens of steps. Three specially picked random cases show different convergence paths.

4.2. Fast convergence compared with SPGD

The neural-network-based iterative method turns out to be a fast-converging method for feedback. For comparison, we ran both the NN algorithm and a widely used Stochastic Parallel Gradient Descent [10] control algorithm on the same simulator. The efficiency versus feedback steps of both methods are shown in Fig. 13, with thirty random runs from random initial states. The majority of the NN based curves converge in about 40 steps (red curves), and can reach to a final efficiency of 99%. The phase dither range and correction gain for the SPGD algorithm (blue curves) are optimized for rapid convergence and high combining efficiency. We find that the number of steps required for SPGD to reach the optimal state is ~ 800, consistent with other published results for SPGD-stabilized beam combination [12], roughly a factor of 10 times number of channels to combine. If combining 81 beams with 1kHz repetition rate, it would take nearly a second to recover from large perturbations, making full suppression of even thermal phase

Optics EXPRESS

errors impossible. Here we only compare with the basic SPGD algorithm. Another approach improves the SPGD algorithm by dithering with an orthogonal basis set, which improves the convergence speed but only by a factor of 2 or 3 [30]. The NN-based pattern recognition phase detection scheme is faster because it starts with more information.

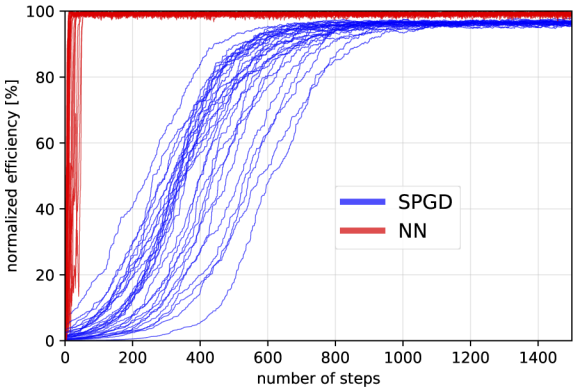

Fig. 13. Comparison of normalized combining efficiency versus number of correction steps using NN algorithm (red curves for 30 random cases) and SPGD (blue curves for 30 random cases).

Also, the SPGD has a lower final efficiency because the SPGD detector only measures the center combined power, where the information for feedback is very limited. This is a cosine function of each beam phase, so that the gradient goes to zero at optimum efficiency. There is also loss of efficiency due to effective averaging near the optimal state: when near optimal, the N-channel combining process reduces the phase detection sensitivity σ_N from uncorrelated RMS error of single channel σ_ϕ as: $\sigma_N = \sigma_\phi/\sqrt{N}$ [21]. Thus the SPGD phase detection sensitivity is inversely proportional to the square root of the number of beams, and the correction gain diminishes due to averaging, which also prevents strong feedback near the optimal state and results in lower final efficiency.

In contrast, our scheme detects all the side beams, many of which have non-zero power gradients at the optimum efficiency point. Thus, our scheme can sense phase with equal sensitivity at any phase state, allowing higher combining efficiency near optimal. The NN pattern recognition scheme is a linear phase detector without dithering.

For the NN based feedback, the convergence speed and the final normalized efficiency is strongly dependent on the NN model's training range. As shown in Fig. 14, we applied several NN models trained in different phase perturbation ranges listed in Table 1. The NN model was trained in $[-20, 20]$ degree (blue curve), $[-40, 40]$ degree (orange curve), $[-60, 60]$ degree (green curve), $[-80, 80]$ degree (red curve). The figure also shows the trajectory of a combined NN model, which uses the 80 degree model when the combining efficiency is less than 80%, then changes to a 40 degree model when the combining efficiency is 80% to 90%, and then finally to a 20 degree model (purple curve). When the training range is larger, the convergence speed is faster while the final efficiency is lower due to a larger RMSE, as also shown in Table 1. Large RMSE introduces noticeable oscillations in the efficiency curve when the phase is corrected in each loop iteration, as shown by the red curve for NN trained in [-80, 80] degree range and with RMSE 14.1 degrees. For other NN models with RMSE within 6 degrees, the oscillation is within 1% efficiency, thus keeping stable within the required tolerance during the iterative process.

Optics EXPRESS

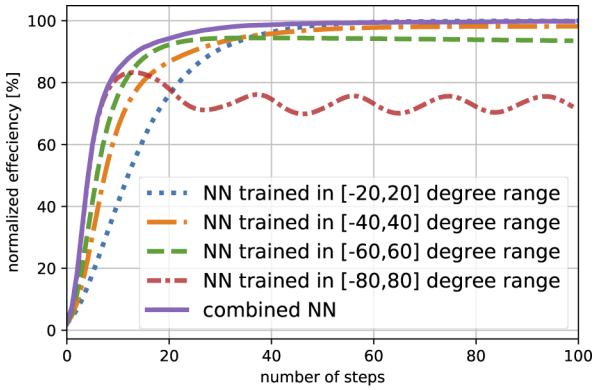

Fig. 14. Normalized combining efficiency versus number of correction steps using neural network based feedback with different NN models, within 100 steps.

4.3. Discussion of stability and bandwidth of the NN based iterative method

Any measurement noise will cause NN prediction uncertainty which would reduce the achievable combining efficiency and convergence speed. We have added realistic camera noise in the testing data set, to compare the performance between NN and SPGD performance as shown in Fig. 13. With the beam power unit as defined in section 2.1, we added random noise of 0.1 RMS to the diffraction pattern, corresponding to 10% of each beam's contribution. It also corresponds to the camera noise observed on the side beams, when the center combined beam is saturated. Our study suggests that the RMS noise level should be less than 30% of the power unit in order to keep the feedback loop stable.

In general, the more accurate the error prediction is, the more robust the feedback will be, as shown in Fig. 14. There are other practical issues that can cause feedback instability [31,32]. In this paper we focus more on beam phase error detection than control loop stability and optimization, thus a simple proportional-only controller is used for feedback simulation. The gain setting for such a controller is tuned to optimize both NN based feedback and SPGD based feedback. The result may serve as a reference for further development of advanced controllers such as linear quadratic estimation (Kalman Filter) control with a greater tolerance for noise [33].

We have also studied the increase in computational resources with increasing numbers of channels to combine. For the 81-beam case, training requires about 500k data samples, but if only combining the center 9 beams, as little as 500 samples are enough. The inference latency for both cases is identical.

Our feedback control needs to suppress acoustic perturbations within a bandwidth of ~ 100 Hz, when the sampling rate (or repetition rate) is in the kHz range. It is feasible to push the inference latency down to <2 milliseconds using a hard-real-time edge computer such as an FPGA [34], compared with ~ 10 milliseconds latency using a CPU.

5. Conclusion

In summary, we have demonstrated a novel neural-network-based iterative method for stabilizing 81-way 2D diffractive laser combination. The neural-network is trained as a phase detector based on pattern recognition of interference patterns emerging from a DOE. Training is in a limited phase perturbation range, and for phase perturbations within the training range it can feedback correct to the optimal state in one step. The neural-network can also be applied to a realistic case of 360 degree full range. Applying iterative feedback, it benefits from downhill random walking at the beginning, speeding up toward convergence rapidly once it steps into the training

Optics EXPRESS

range. The neural-network-based iterative method converges tens of times faster than the SPGD with a single-detector and an algorithm with random dither, which requires hundreds of steps to converge. This method is applicable to high power CW as well as ultrafast pulse combination, compensating for thermal and mechanical perturbations. For our purposes, these results enable kHz, ultrafast pulsed laser beam combination with an arbitrarily large number of beams, for scaling to high energy.

Funding. High Energy Physics (DEAC02–05CH11231).

Acknowledgments. This work was supported by the Early Career Research Program of U.S. Department of Energy, and the Laboratory Directed Research and Development Program of Lawrence Berkeley National Laboratory, under U.S. Department of Energy Contract No. DE-AC02–05CH11231.

Disclosures. The authors declare no conflicts of interest.

References

1. D. J. Richardson, J. Nilsson, and W. A. Clarkson, "High power fiber lasers: current status and future perspectives," J. Opt. Soc. Am. B **27**(11), B63–B92 (2010).
2. M. N. Zervas and C. A. Codemard, "High power fiber lasers: a review," IEEE J. Sel. Top. Quantum Electron. **20**(5), 219–241 (2014).
3. W. Leemans, Laser technology for k-bella and beyond, Tech. rep., Technical Report, Lawrence Berkeley National Laboratory (2017).
4. R. Falcone, F. Albert, F. Beg, S. Glenzer, T. Ditmire, T. Spinka, and J. Zuegel, Workshop report: Brightest light initiative, Tech. rep., OSA Headquarters, Washington, D.C, United States (2019).
5. T. Zhou, T. Sano, and R. Wilcox, "Coherent combination of ultrashort pulse beams using two diffractive optics," Opt. Lett. **42**(21), 4422–4425 (2017).
6. T. Zhou, Q. Du, T. Sano, R. Wilcox, and W. Leemans, "Two-dimensional combination of eight ultrashort pulsed beams using a diffractive optic pair," Opt. Lett. **43**(14), 3269–3272 (2018).
7. R. Wilcox, "Optical pulse combiner comprising diffractive optical elements," (2019). US Patent 10, 444, 526.
8. S. J. Augst, T. Fan, and A. Sanchez, "Coherent beam combining and phase noise measurements of ytterbium fiber amplifiers," Opt. Lett. **29**(5), 474–476 (2004).
9. J. Anderegg, S. Brosnan, E. Cheung, P. Epp, D. Hammons, H. Komine, M. Weber, and M. Wickham, "Coherently coupled high-power fiber arrays," in *Fiber Lasers III: Technology, Systems, and Applications*, vol. 6102 (International Society for Optics and Photonics, 2006), p. 61020U.
10. M. A. Vorontsov and V. Sivokon, "Stochastic parallel-gradient-descent technique for high-resolution wave-front phase-distortion correction," J. Opt. Soc. Am. A **15**(10), 2745–2758 (1998).
11. C. Yu, S. Augst, S. Redmond, K. Goldizen, D. Murphy, A. Sanchez, and T. Fan, "Coherent combining of a 4 kw, eight-element fiber amplifier array," Opt. Lett. **36**(14), 2686–2688 (2011).
12. P. Zhou, Z. Liu, X. Wang, Y. Ma, H. Ma, X. Xu, and S. Guo, "Coherent beam combining of fiber amplifiers using stochastic parallel gradient descent algorithm and its application," IEEE J. Sel. Top. Quantum Electron. **15**(2), 248–256 (2009).
13. Q. Du, T. Zhou, L. R. Doolittle, G. Huang, D. Li, and R. Wilcox, "Deterministic stabilization of eight-way 2d diffractive beam combining using pattern recognition," Opt. Lett. **44**(18), 4554–4557 (2019).
14. J. R. Fienup, "Phase retrieval algorithms: a comparison," Appl. Opt. **21**(15), 2758–2769 (1982).
15. H. Tünnermann and A. Shirakawa, "Deep reinforcement learning for coherent beam combining applications," Opt. Express **27**(17), 24223–24230 (2019).
16. J. White and Z. Chang, "Attosecond streaking phase retrieval with neural network," Opt. Express **27**(4), 4799–4807 (2019).
17. D. Wang, Q. Du, T. Z. B. Mohammed, M. Kiran, D. Li, and R. Wilcox, "Artificial neural networks applied to stabilization of 81-beam coherent combining," in *2020 OSA Laser Congress*, (2020), p. ATu4A.6.
18. Q. Du, D. Wang, T. Zhou, D. Li, and R. Wilcox, "Characterization and control for 81-beam diffractive coherent combining," in *2020 OSA Laser Congress*, (2020), p. ATu4A.5.
19. Q. Du, D. Wang, T. Zhou, D. Li, and R. Wilcox, "Stabilization of 81-channel coherent beam combination usingmachine learning," Opt. Express (to be published) (2021).
20. J. R. Leger, G. J. Swanson, and W. B. Veldkamp, "Coherent laser addition using binary phase gratings," Appl. Opt. **26**(20), 4391–4399 (1987).
21. G. D. Goodno, C.-C. Shih, and J. E. Rothenberg, "Perturbative analysis of coherent combining efficiency with mismatched lasers," Opt. Express **18**(24), 25403–25414 (2010).
22. T. Hou, Y. An, Q. Chang, P. Ma, J. Li, L. Huang, D. Zhi, J. Wu, R. Su, Y. Ma, and P. Zhou, "Deep learning-based phase control method for coherent beam combining and its application in generating orbital angular momentum beams," *>arXiv preprint arXiv:1903.03983* (2019). Available at Ohttps://arxiv.org/abs/1903.03983.
23. H. Tünnermann and A. Shirakawa, "Deep reinforcement learning for tiled aperture beam combining in a simulated environment," JPhys Photonics **3**(1), 015004 (2021).

Optics EXPRESS

24. J. Brownlee, "How to configure the number of layers and nodes in a neural network," (2019). https://machinelearningmastery.com/how-to-configure-the-number-of-layers-and-nodes-in-a-neural-network/.
25. I. V. Tetko, D. J. Livingstone, and A. I. Luik, "Neural network studies. 1. comparison of overfitting and overtraining," J. Chem. Inf. Model. **35**(5), 826–833 (1995).
26. A. Tsoularis and J. Wallace, "Analysis of logistic growth models," Math. Biosci. **179**(1), 21–55 (2002).
27. M. I. Jordan, Why the logistic function? a tutorial discussion on probabilities and neural networks, Tech. rep., Massachusetts Institute of Technology (1995).
28. E. Biganzoli, P. Boracchi, L. Mariani, and E. Marubini, "Feed forward neural networks for the analysis of censored survival data: a partial logistic regression approach," Statist. Med. **17**(10), 1169–1186 (1998).
29. A. Allam, M. Nagy, G. Thoma, and M. Krauthammer, "Neural networks versus logistic regression for 30 days all-cause readmission prediction," Sci. Rep. **9**(1), 9277 (2019).
30. A. Brignon, *Coherent laser beam combining* (John Wiley & Sons, 2013).
31. G. Ellis, *Observers in control systems: a practical guide* (Elsevier, 2002).
32. G. C. Goodwin, S. F. Graebe, and M. E. Salgado, *Control system design* (Prentice Hall, Upper Saddle River, NJ, 2001).
33. G. Welch and G. Bishop, *An introduction to the Kalman filter* (Chapel Hill, NC, USA, 1995).
34. "Xilinx. zynq dpu v3.2 ip product guide," (2020). https://www.xilinx.com/support/documentation/ip_documentation/dpu/v3_2/pg338-dpu.pdf.